

EFFECTIVE QUANTIZATION OF MUON OPTIMIZER STATES

Aman Gupta,* Rafael Celente,* Abhishek Shivanna,* D. T. Braithwaite*

Nubank

{aman.gupta, rafael.celente}@nubank.com.br

{abhishek.shivanna, daniel.braithwaite}@nubank.com.br

Gregory Dexter,* Shao Tang*

LinkedIn

{gdexter, shatang}@linkedin.com

Hiroto Udagawa, Daniel Silva, Rohan Ramanath, S. Sathiya Keerthi

Nubank

ABSTRACT

The Muon optimizer, based on matrix orthogonalization, has recently shown faster convergence and up to 2x computational efficiency over AdamW in LLM pretraining. Like AdamW, Muon is stateful, requiring storage of both model weights and accumulated gradients. While 8-bit AdamW variants mitigate this overhead using blockwise quantization, they are typically stable only under dynamic quantization - which improves stability on linear quantization for extreme values. In this paper, we introduce the 8-bit Muon optimizer using blockwise quantization, supporting both linear and dynamic schemes. We demonstrate that 8-bit Muon maintains stability under both, while delivering $\sim 74\%$ reduction in memory footprint compared to full-precision Muon. In extensive experiments, 8-bit Muon closely matches the performance of Muon while outperforming AdamW and 8-bit AdamW in pre-training a 1.6B model on 4B FineWeb tokens. It also shows competitive results when fine-tuning the Llama 3.2 3B model on post-training data. We also provide a theoretical perspective to help explain this robustness under quantization.

1 INTRODUCTION

Scaling laws for large language models (LLMs) (Kaplan et al., 2020; Hoffmann et al., 2022) indicate that larger models generally achieve better out-of-distribution performance across diverse tasks. Yet, GPU high-bandwidth memory (HBM) capacity has not kept pace with parameter counts. During training, memory is dominated by model parameters, gradients, optimizer states, and activations. Systems work has therefore focused on distributing these tensors across devices via distributed data parallel (DDP), Fully Sharded Data Parallel (FSDP) (Zhao et al., 2023), ZeRO stage-3 in DeepSpeed (Rajbhandari et al., 2020), and tensor/model parallelism (Shoeybi et al., 2019) in order to improve inference performance.

Orthogonal to sharding is compressing the optimizer state. AdamW (Loshchilov & Hutter, 2017; Kingma, 2014), the *de facto* optimizer for LLMs, maintains two FP32 moment buffers (first and second moments) per parameter. For an 8B-parameter model (e.g., an 8B Llama-3 variant (Dubey et al., 2024)), this alone occupies 64 GB ($\sim 80\%$ of an NVIDIA H100's 80 GB HBM), leaving little headroom for parameters, gradients, and activations. To mitigate this, Dettmers et al. (2021) quantize Adam's optimizer states to 8 bits via block-wise *dynamic* (non-linear) quantization, preserving stability in the presence of extreme values while reducing optimizer memory by roughly 4x — enabling performant training under tight memory budgets.

*Equal contribution.

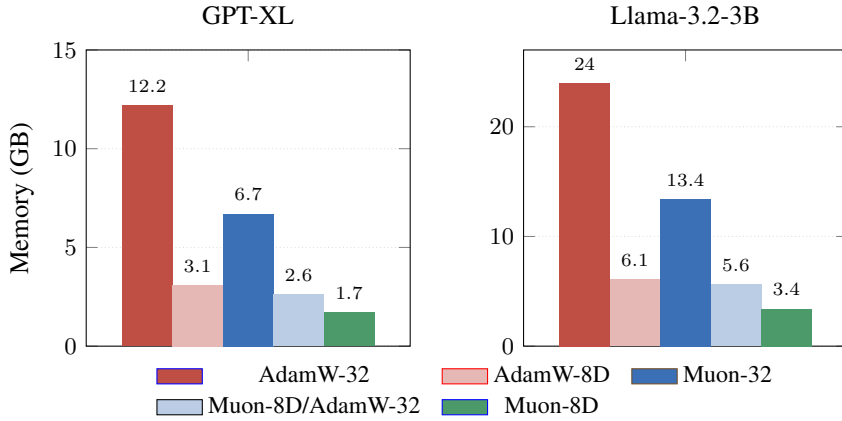


Figure 1: Optimizer state memory (GB) for GPT-XL (1.6B) and Llama-3.2-3B. Muon-8D reduces optimizer state for the GPT-XL and Llama models by as much as **86%** when compared to AdamW-32, and **74%** when compared to Muon-32. Table 1 defines the different variants in the legend.

Recently, there has been a surge of interest in moving beyond AdamW to improve training efficiency (Anil et al., 2020; Shazeer & Stern, 2018; Vyas et al., 2024). Among various advances, one particularly promising optimizer is **Muon** (Jordan et al., 2024)¹, which orthogonalizes the gradient momentum before updating the parameters. Equalizing the importance of all update directions results in improved stability and better convergence (Bernstein & Newhouse, 2024a; Bernstein, 2025). Several large-scale studies have confirmed Muon’s ability to achieve a 2x efficiency in a target validation loss compared to AdamW on a compute-optimal setup (Liu et al., 2025; Shah et al., 2025). This includes extremely large models up to a trillion parameters, such as Kimi K2 (Team et al., 2025) and GLM4.5 (Zeng et al., 2025).

In this paper, we introduce the **8-bit Muon** optimizer with blockwise quantization. While 8-bit AdamW variants are usually stable only using dynamic quantization, we demonstrate that **8-bit Muon can handle both linear and dynamic quantization effectively**. Our contributions can be summarized as:

- We study 8-bit AdamW, and pinpoint the source of its instability with linear quantization. Surprisingly, we also discover that SGD with momentum² and its closely related algorithm Muon are robust to linear quantization, achieving close to generalization parity when compared to their full-precision counterparts. **We also provide a theoretical perspective to explain SGD’s and Muon’s robustness under quantization..**
- We **propose and evaluate several 8-bit variants of the Muon optimizer**, systematically applying both linear and dynamic quantization of Muon to hidden matrix-valued parameters and AdamW to the remaining parameters. Table 1 describes all the variants.
- **For pre-training** models up to 1.6B parameters, our 8-bit Muon variants, regardless of the quantization scheme used for the Muon-associated parameters, are highly effective, **achieving a validation loss within 1%-2% of the full-precision Muon optimizer for smaller models and matching its performance for the 1.6B model**, while consistently outperforming all AdamW baselines.
- **For fine-tuning**, we train the Llama 3.2 3B model (Dubey et al., 2024) on splits of the *tulu-3-sft-mixture* post-training dataset (Lambert et al., 2024). **8-bit Muon demonstrates competitive performance when compared to Muon, AdamW and 8-bit AdamW variants.**
- Our 8-bit Muon variants reduce the optimizer state memory substantially. For the 1.6B model, an 8-bit variant has a state that is smaller by up to **~86% compared to AdamW**

¹Muon is closely related to SGD with momentum, adding a per-layer matrix orthogonalization

²Throughout, we use SGD to mean SGD with momentum, unless otherwise noted.

Model	Muon state	AdamW state	Shorthand
32-bit AdamW	—	32b	AdamW-32
32-bit Muon	32b	32b	Muon-32
8-bit AdamW (dynamic)	—	8b D	AdamW-8D
8-bit Muon (dynamic), 8-bit AdamW	8b D	8b D	Muon-8D
8-bit Muon (linear), 8-bit AdamW	8b L	8b L	Muon-8L
8-bit Muon (dynamic), 32-bit AdamW	8b D	32b	Muon-8D/AdamW-32
8-bit Muon (linear), 32-bit AdamW	8b L	32b	Muon-8L/AdamW-32

Table 1: Optimizer variants considered for pre-training and SFT. D = dynamic quantization, L = linear quantization. 8-bit Muon has 4 variants.

(Muon-8D vs. AdamW-32), ~74% compared to Muon (Muon-8D vs. Muon-32) and ~44% compared to 8-bit AdamW (Muon-8D vs. AdamW-8D); enabling efficient training of large models. We achieve a similar reduction in optimizer state for SFTing the Llama 3.2 3B model, **reducing the optimizer state footprint from ~24 GB (AdamW-32) to ~3.4 GB (Muon-8D)** (Figure 1).

2 RELATED WORK

Efficient Optimizers There has been some prior work on alleviating the memory cost of training with optimizers like AdamW. Techniques like low-rank adaptation (LoRA) (Hu et al., 2022) allow a small subset of parameters to be fine-tuned for downstream tasks, but often fall behind in quality when compared to full parameter fine-tuning (Biderman et al., 2024). Adafactor (Shazeer & Stern, 2018) factorizes the second moment for matrices, reducing memory consumption compared to AdamW. Dettmers et al. (2021) introduced the 8-bit Adam optimizer, but it only works when combined with careful blockwise + dynamic quantization. Adam Galore (Zhao et al., 2024) leverages the low-rank structure of the gradients to reduce state size and can be combined with state quantization. Our work is directly comparable to Dettmers et al. (2021)’s work, and can potentially be combined with low-rank updates.

Gradient Orthogonalization The Muon optimizer (Jordan et al., 2024) has sparked interest in algorithms that take advantage of the orthonormalization of the gradient of matrix-valued parameters. Muon makes each weight matrix update orthonormal through polar decomposition (Newton-Schulz), giving direction-only, spectrally controlled steps for hidden layers. To scale it to large LLMs, recent works add decoupled weight decay and careful per-parameter update scaling (Liu et al., 2025). Dion (Ahn et al., 2025) leverages orthonormalization but is built for distributed training: using low-rank orthonormalization with device-local momentum/error-feedback to avoid reconstruction or synchronization of full matrices.

Quantization Quantization is a versatile tool for managing the memory cost of training large models. While we apply quantization to the state of the Muon optimizer, it has also been successfully applied to model weights in two settings - post-training quantization (PTQ) and quantization-aware training (QAT). PTQ uses calibration data to quantize the weights of large models in one shot to k bits, where k can be as low as 1 or 2 (Tseng et al., 2024; Frantar et al., 2022; Lin et al., 2024; Behdin et al., 2023). QAT involves training with quantized weights (Liu et al., 2023). Both PTQ and QAT require hardware support to realize the full benefits of quantization. Another interesting work is MuLoCo (Thérien et al., 2025), where the authors apply Muon as the inner (local) optimizer in a DiLoCo-style (Douillard et al.) loop, geared toward compressing parameter updates during distributed training. Thus, MuLoCo/DiLoco use quantization only for gradient updates.

3 BACKGROUND

3.1 QUANTIZATION FOR OPTIMIZERS

Quantization is the process of reducing the precision of numerical representations by mapping a value expressed in a richer way into a simpler one. For example, representing a real number as a 32-bit floating-point value, or converting a 32-bit float into an 8-bit integer, are both forms of

quantization. In deep learning, model parameters and optimizer states are typically stored as 32-bit floating-point numbers, making their conversion to lower-precision formats a primary goal of quantization.

For instance, linear quantization is a method (among many) to quantize the state tensor \mathbf{X} of an optimizer from 32-bit floats to 8-bit integers. This involves (a) dividing all the floats in the tensor by the absolute max to get a normalization constant $S = \max(|\mathbf{X}|)$ and (b) mapping the normalized value to the integer i in the range -127 to 127 , using uniform spacing of the normalized values in $[-1, 1]$, written as $i = \text{round}(\frac{\mathbf{X}}{S} \times 127)$. Dequantization then converts the codebook index back by multiplying with the previously stored normalization constant to recover $\tilde{\mathbf{X}} = \frac{S}{127} \times i$.

For 8-bit quantization, the number of addressable states is 256. Dettmers et al. (2021) discuss another quantization codebook design - dynamic quantization. Dynamic quantization is a more sophisticated approach that quantizes non-uniformly by allocating more codes to regions with high densities and fewer codes to sparsely used regions. This increases resilience to non-uniform data.

A crucial recipe for reducing the effect of outliers is blockwise quantization (Dettmers et al., 2021), where one can segment a tensor into one or more blocks, and then perform quantization (linear, dynamic, or other schemes) separately within each block. A nice side effect of blockwise quantization is that each block can be processed in parallel. For a more detailed treatment of blockwise and dynamic quantization, please refer to (Dettmers et al., 2021).

3.2 THE MUON ALGORITHM

The Muon update on a single hidden layer can be described as follows:

$$\begin{aligned} \mathbf{M}^{(t)} &:= \beta \mathbf{M}^{(t-1)} + \nabla f_t(\mathbf{W}^{(t-1)}), \\ \mathbf{U}^{(t)} &:= \text{NS}(\mathbf{M}^{(t)}), \\ \mathbf{W}^{(t)} &:= \mathbf{W}^{(t-1)} - \alpha \mathbf{U}^{(t)}. \end{aligned} \tag{1}$$

where t is the iteration number and \mathbf{M} is the momentum of the gradient. NS stands for the Newton-Schulz iteration process (Bernstein & Newhouse, 2024b; Higham, 2008), used to find an approximation for $\mathbf{U}\mathbf{V}^T$ where $\mathbf{U}\Sigma\mathbf{V}^T$ is the singular value decomposition (SVD) of \mathbf{M} . Orthogonalization equalizes the importance of each update direction by collapsing all singular values to 1.

The vanilla version of Muon described above does not use weight decay. Additionally, it is not obvious whether it requires any hyperparameter tuning over AdamW baselines. Liu et al. (2025) introduced a variant of Muon that uses weight decay and also scales its update to match the update RMS of AdamW, producing the following version:

$$\begin{aligned} \mathbf{M}^{(t)} &:= \beta \mathbf{M}^{(t-1)} + \nabla f_t(\mathbf{W}^{(t-1)}), \\ \mathbf{U}^{(t)} &:= \text{NS}(\mathbf{M}^{(t)}), \\ \mathbf{W}^{(t)} &:= \mathbf{W}^{(t-1)} - \alpha (0.2 \cdot \mathbf{U}^{(t)} \cdot \sqrt{\max(m, n)} + \lambda \mathbf{W}^{(t)}). \end{aligned} \tag{2}$$

where m and n are the dimensions of \mathbf{M} . Liu et al. (2025) claim that with Eq 2, hyperparameters such as learning rate and weight decay can be shared across matrix and non-matrix parameters. In the rest of the paper, any mention of Muon refers to the version in Equation 2, unless stated otherwise. It is important to note that any non-matrix parameters and input/output parameters are optimized using AdamW, leaving Muon to focus on matrix-valued hidden parameters. Complete algorithms can be found in Appendix B.

4 METHODS

4.1 WHY IS 8-BIT ADAMW UNSTABLE UNDER LINEAR QUANTIZATION?

Dettmers et al. (2021) observed that naïve 8-bit *linear* quantization performs poorly because it allocates too little resolution to small-magnitude entries, yielding large relative errors precisely where

optimizer states concentrate most of their mass. We make this behavior concrete in Theorem 1 by analyzing how quantization error propagates and is magnified through the second-moment accumulator v . In particular, we show that if moderate-size gradient coordinates occur with non-negligible probability, then the expected squared error of one step of Adam with linearly quantized states *diverges* as the numerical stabilizer $\epsilon \rightarrow 0$. The result holds for standard Adam hyperparameters; constants are kept explicit to emphasize practical regimes (e.g., $\epsilon \approx 10^{-8}$) where the error is already proved to be orders of magnitude larger than the unquantized update norm.

Let Q denote the 8-bit linear quantization operator from Definition 1. We analyze the base Adam algorithm without weight decay³. The quantized variant applies Q to the moment estimates before forming the update. All algorithmic details, definitions, and proofs are provided in Appendix C.

Theorem 1 *Let $\theta^{(1)}$ denote the parameters after one step of Adam as given in Algorithm 4, and let $\tilde{\theta}^{(1)}$ denote the parameters after one step of the same algorithm with 8-bit linear quantization applied to the moment estimates (Definition 1), i.e.:*

$$\tilde{\theta}^{(1)} = \theta^{(0)} - \alpha \cdot \frac{Q(\mathbf{m}^{(1)})}{\sqrt{Q(\mathbf{v}^{(1)})} + \epsilon}.$$

Suppose that each entry of $\mathbf{g}^{(1)} \in \mathbb{R}^d$ satisfies $\mathbb{P}\left(\frac{\|\mathbf{g}\|_\infty}{60} < |\mathbf{g}_i| < \frac{\|\mathbf{g}\|_\infty}{16}\right) \geq \nu$ and $\|\mathbf{g}\|_\infty \geq g_\infty > 256\epsilon$ with probability one. Then

$$\mathbb{E} \|\theta^{(1)} - \tilde{\theta}^{(1)}\|_2^2 \geq \frac{d\nu\alpha^2 g_\infty^2}{(256\epsilon)^2}.$$

4.2 THE CURIOUS CASE OF 8-BIT SGD WITH MOMENTUM

The proof of Theorem 1 shows that the instability of Adam with linear quantization arises primarily from error in the second-moment vector, which appears in the denominator of the update rule. This naturally raises the question: **does 8-bit linear quantization suffice when such a denominator is avoided?**

From a theoretical perspective, we show that, unlike Adam, SGD with momentum admits a uniform error bound under linear quantization. In particular, for any initialization of the weights and momentum, the quantization error remains bounded. Let $\eta > 0$ denote the step size and $\rho \in [0, 1)$ the momentum parameter.

Theorem 2 *Consider a step of SGD with momentum with and without 8-bit linear quantization of the momentum:*

$$\tilde{\theta}^{(t+1)} = \theta^{(t)} - \eta(\mathbf{g}^{(t)} + \rho Q(\mathbf{m}^{(t)})) \text{ and } \theta^{(t+1)} = \theta^{(t)} - \eta(\mathbf{g}^{(t)} + \rho \mathbf{m}^{(t)}).$$

From any point $\theta^{(t)}$ and any momentum state $\mathbf{m}^{(t)}$, if Q is as in Definition 1, then

$$\|\tilde{\theta}^{(t+1)} - \theta^{(t+1)}\|_2^2 \leq d\eta^2 \rho^2 \left(\frac{\|\mathbf{m}^{(t)}\|_\infty}{127} \right)^2.$$

Empirically, we confirm this difference. We train a ResNet-50 model (He et al., 2016) on the ImageNet dataset (Deng et al., 2009), using a standard training regime of 90 epochs. We compare AdamW and variants of SGD with momentum. Results are in Table 2. **Surprisingly, SGD with linear 8-bit quantization achieves the same high validation top-1 accuracy (Goyal et al., 2017) of 76%+ as full-precision SGD.** AdamW underperforms when compared to SGD (a well-known result on image classification training), while AdamW with linear quantization diverges immediately. See Appendix A.1.1 for extended details.

Together, these theoretical and empirical results demonstrate that the instability of quantized Adam is specifically driven by the quantization of the second-moment term in the denominator.

³The result extends immediately to AdamW, since the decay of $\theta^{(0)}$ affects both $\tilde{\theta}^{(1)}$ and $\theta^{(1)}$ equally and therefore cancels out.

Method	SGD+M	AdamW
FP32	76.21	74.42
8-bit linear quant.	76.25	—

Table 2: Top-1 validation accuracy (%) after 90 epochs for SGD+M and AdamW in FP32 and with 8-bit linear quantization. “—” indicates that Adam with linear quantization diverged.

4.3 THE 8-BIT MUON ALGORITHM

Since SGD works well with linear quantization, we now propose 8-bit quantized variants for the Muon algorithm that leverage either linear or dynamic schemes. In Table 1, we introduce various variants of Muon and AdamW that leverage different quantization schemes. Since Muon uses orthogonalization only for hidden matrix-valued parameters, the other parameters like embeddings and classifier heads are usually optimized with AdamW. The variants listed in Table 1 consist of linear, dynamic, and even hybrid versions.

The 8-bit Muon update can be written as:

$$\begin{aligned}
\widetilde{\mathbf{M}}^{(t-1)} &:= \text{DQ}_B^{\text{mode}}(\mathbf{Z}^{(t-1)}, \mathcal{S}^{(t-1)}), \\
\mathbf{M}^{(t)} &:= \beta \widetilde{\mathbf{M}}^{(t-1)} + \nabla f_t(\mathbf{W}^{(t-1)}), \\
\mathbf{U}^{(t)} &:= \text{NS}(\mathbf{M}^{(t)}), \\
\mathbf{W}^{(t)} &:= (1 - \alpha \lambda) \mathbf{W}^{(t-1)} - 0.2 \alpha \sqrt{\max(m, n)} \mathbf{U}^{(t)}, \\
(\mathbf{Z}^{(t)}, \mathcal{S}^{(t)}) &:= \text{Q}_B^{\text{mode}}(\mathbf{M}^{(t)}).
\end{aligned} \tag{3}$$

where \mathbf{Z} refers to the compressed momentum buffer and \mathcal{S} is the associated state required to dequantize it. Q_B^{mode} is the quantization function, and $\text{DQ}_B^{\text{mode}}$ dequantizes the compressed momentum vector for use in the update. Rest of the notation is borrowed from Equation 2. The complete algorithms for 8-bit Muon can be found in Appendix B.

We now claim that like SGD, even Muon admits a uniform bound under linear quantization. In fact, in Theorem 3 we show the following: when Muon uses an exact orthogonalization procedure (via the SVD), the quantization error bound for a single layer matches the SGD case up to an additional dependence on the smallest singular value, s , of the momentum matrix. This dependence is natural, since the conditioning of the momentum controls the stability of the orthogonal factor. In practice, the margin s is typically not small, so the guarantee has the same qualitative form as the SGD result.

Theorem 3 *Consider a step of Muon with momentum (using the exact polar factor rather than the Newton–Schulz approximation) with and without 8-bit linear quantization of the momentum. Let the layer weights and momentum state be $\mathbf{W}^{(t-1)}$ and $\mathbf{M}^{(t-1)}$, each with d entries (see Appendix C.4 for full update formulas).*

Suppose that, after a single gradient update, both the original and quantized momentum matrices are full column rank with minimum singular value at least $s > 0$. Then

$$\|\widetilde{\mathbf{W}}^{(t)} - \mathbf{W}^{(t)}\|_{\text{F}}^2 \leq \frac{d\alpha^2\beta^2}{s^2} \left(\frac{\|\text{vec}(\mathbf{M}^{(t-1)})\|_{\infty}}{127} \right)^2,$$

where $\widetilde{\mathbf{W}}^{(t)}$ denotes the weights after the quantized update and $\mathbf{W}^{(t)}$ after the unquantized update.

5 EXPERIMENTS

5.1 PRE-TRAINING WITH 8-BIT MUON

Architectures For the pre-training task, we train from scratch a modified version of the GPT2 architecture (Radford et al., 2019) in which the learned positional embeddings are replaced by rotary

positional embeddings (RoPE) (Su et al., 2024). To understand the scaling effect, we consider 4 different sizes - XS (97M), Small (124M), Medium (405M) and XL (1.6B). For the sake of brevity, we will refer to this architecture as GPT in the rest of the paper. Detailed notes on the architecture can be found in Table 6 in Appendix A.1.2.

Datasets Our pre-training dataset consists of 2 billion tokens from the FineWeb-Edu dataset Penedo et al. (2024) for the XS, Small and Medium models, and 4 billion tokens for the XL model. To achieve this, we take twenty (forty for the XL variant) chunks of the dataset, each chunk being approximately 100M tokens. We use 50k samples from the validation split of FineWeb to measure validation loss, totaling approximately 100M tokens.

Training details We pre-train the 4 GPT models from scratch using the splits from FineWeb described earlier. For AdamW, we set β_1 and β_2 to 0.9 and 0.999 respectively. The ϵ value for AdamW variants is set to 10^{-8} . For Muon, we set the momentum parameter to 0.95.

The block size of the quantized versions of AdamW and Muon is set to 2048. We use the bitsandbytes library (Dettmers et al., 2023) for quantization / dequantization routines for linear and dynamic quantization. We fix decoupled weight decay to 0.1 for all experiments.

We use the WSD learning rate schedule (Hu et al., 2024), with a linear warm up of the learning rate from 0 to the peak in 10% of training steps, a linear decay to zero in the last 10% steps. For XS, Small and Medium models, we fix the peak learning rate to 3×10^{-4} for all variants. For the XL model, we reduced the maximum learning rate to 2×10^{-4} for all variants. Since most of the peak learning rates have been tuned for AdamW, we make no attempt to tune the peak learning rate for Muon and its variants, since **our version of Muon is supposed to be a drop-in replacement for AdamW without any requirement to tune learning rate or weight decay** (Liu et al., 2025).

We use distributed data parallel (DDP) for all experiments, with training working on multiple GPUs at the same. Our largest model is 1.6B and fits on a single NVIDIA H100 GPU. The global batch size is fixed at 262k tokens, and is achieved with varying gradient accumulation across model sizes. A detailed table on hyperparameters and training configurations can be found in Appendix A.1.2.

Evaluation criteria We use validation loss as the primary criterion for comparing performance for pre-training. We exhibit results from a single representative run of each experimental variant since the variance across runs was low.

5.1.1 RESULTS

Investigating the stability of 8-bit Muon optimizers In Figure 2, we show the results of comparing all variants of 8-bit Muon described in Table 1 on the task of pre-training the GPT-Medium model. **Before testing these variants, we confirmed that AdamW-8L diverged on this problem early during training.** Interestingly, Muon-8L did not diverge, but performed poorly. Remarkably, all other versions of 8-bit Muon closely match each other. This includes Muon-8L/Adam-32, a version that uses linear quantization for Muon-associated parameters. **This corroborates our theoretical findings that AdamW is particularly unstable especially when using simple techniques like linear quantization. Because of these findings, we avoid the Muon-8L variant and instead use alternatives like Muon-8L/Adam-32.**

The main results can be found in Figure 3 and Table 3. We make the following observations:

Muon outperforms AdamW variants Unsurprisingly, Muon outperforms all variants of AdamW. This is despite no tuning of the peak learning rate or weight decay.

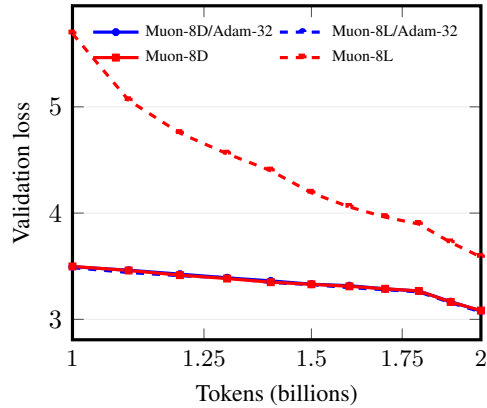


Figure 2: Training curves on GPT-Medium comparing four variants of 8-bit Muon (zoomed in version, from 1B to 2B tokens). Except Muon-8L, all the others follow each other closely.

Model	AdamW-32	AdamW-8D	Muon-32	M-8L/A-32		M-8D/A-32		M-8D	
				loss	(% close)	loss	(% close)	loss	(% close)
XS	3.509	3.499	3.325	3.359	1.02	3.362	1.10	3.364	1.16
Small	3.406	3.489	3.192	3.228	1.14	3.232	1.25	3.233	1.28
Medium	3.269	3.624	3.030	3.070	1.32	3.078	1.61	3.082	1.68
XL	2.994	3.020	2.837	2.830	-0.25	2.822	-0.53	2.803	-1.20

Table 3: Final validation loss for pre-training across models and optimizers. M = Muon, A = Adam. All 8-bit Muon variants are within $\sim 1 - 2\%$ of Muon’s loss, and outperform all AdamW variants comprehensively. For XL, they match the performance of Muon.

8-bit Muon variants are competitive with Muon Surprisingly, all the 8-bit variants of Muon achieve a loss within a $\sim 1\% - 2\%$ error margin of Muon for XS/Small/Medium, comfortably outperforming AdamW-32 and Adam-8D. This includes Muon-8L/Adam-32, which uses linear quantization for hidden matrix-valued parameters. For the XL model, the 8-bit Muon variants match the performance of Muon. **These results show that Muon is robust to the underlying quantization scheme for state compression.**

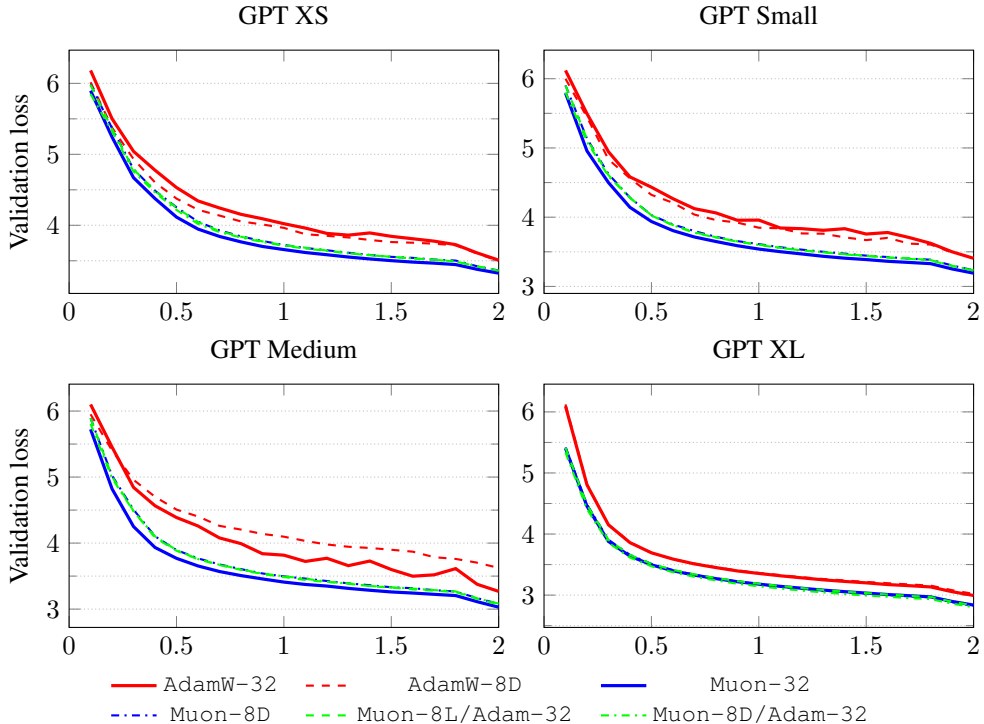


Figure 3: Validation loss for GPT XS/Small/Medium/XL across six optimizers. X-axis: token count (billions). 8-bit Muon optimizers are competitive with Muon, closely matching its performance.

5.2 FINE-TUNING WITH 8-BIT MUON

Architectures We use the Llama 3.2 3B base model (Dubey et al., 2024) for all our fine-tuning (SFT) experiments. It is empirically well-known that if a model is pre-trained with one optimizer, then empirically it is best to fine-tune it with the same optimizer Liu et al. (2025); Team et al. (2025). **Our aim is to assess how closely quantized versions of AdamW and Muon can match their full precision counterparts, and not to achieve state-of-the-art results.**

Model (GPT)	Adam-32	Adam-8D	Muon-32	M-8L/A-32	M-8D/A-32	M-8D
GS8K	28.300 _{0.61}	29.160 _{0.42}	28.050 _{0.425}	28.660 _{0.619}	28.253 _{0.57}	28.730 _{0.35}
HumanEval	26.630 _{0.70}	27.640 _{1.86}	26.420 _{0.93}	27.640 _{0.35}	26.830 _{0.61}	26.950 _{1.17}

Table 4: Llama 3.2 3B SFT Results after lightweight training. Standard deviation across 5 runs is shown in subscript 8-bit variants are competitive with their 32-bit versions.

Datasets We use the `tulu-3-sft-mixture` dataset (Lambert et al., 2024) - an open dataset for post-training which targets a diverse set of skills such as reasoning and math. The dataset consists of close to 1 million training samples.

Training Details We use SFT on the Llama model using all the optimizers used for pre-training. For each optimizer, we use a random 10k split samples from the full Tulu-3 dataset to perform lightweight fine-tuning, since our aim is to compare optimizers in a fair setting. This data-constrained setup is ideal for our aim of comparing optimizers across varying training regimes. Since SFT of LLMs can have non-negligible variance, we conduct 5 runs per experiment.

We inherit all the optimizer setup from pre-training, except for learning rate and weight decay. Learning rate follows a linear warmup to 10^{-5} for the first 3% steps, followed by linear decay to 0. Weight decay is set to 0.01. We use a single NVIDIA H100 GPU for all experiments, with a batch size of 2 and gradient accumulation of 8, yielding a global batch size of 16 sequences.

Evaluation Criteria Our SFT evaluation is performed on the two benchmarks: HumanEval(pass@1) (Chen et al., 2021) for coding and GSM8K (Cobbe et al., 2021) for math.

5.2.1 RESULTS

SFT results can be found in Table 4. Again, the 8-bit variants of Muon match the performance of the 32-bit version. Since Llama 3.2 3B is pre-trained with AdamW, there is no clear winner between AdamW and Muon, mirroring findings from other papers (Liu et al., 2025; Team et al., 2025). We expect Muon-based fine-tuning to be increasingly beneficial as more models pre-trained with Muon are released.

5.3 MEMORY FOOTPRINT

Table 5 compares the persistent HBM memory footprint of the optimizer state for variants, when profiled for the GPT Small, Medium and XL models, as well as Llama-3.2-3B Grattafiori et al. (2024) (Figure 1 summarizes the same info for XL and Llama). For the biggest models like XL and Llama, Muon-8D provides substantial relative savings of $\sim 74\%$, $\sim 86\%$ and $\sim 44\%$, when compared to Muon-32, AdamW-32 and AdamW-8D respectively.

Model	Adam-32	Adam-8D	Muon-32	M-8D/A-32	M-8D
XS	0.73	0.19	0.58	0.47	0.15
Small	1.22	0.31	0.90	0.66	0.23
Medium	3.02	0.77	1.89	1.05	0.47
XL	12.19	3.10	6.69	2.58	1.68
Llama-3.2-3B	23.94	6.10	13.44	5.58	3.37

Table 5: Optimizer states memory (GB) across all model sizes tested (lower is better). Muon-8D reduces optimizer memory footprint for GPT XL and Llama substantially.

For smaller models, Muon-8D/Adam-32 has a larger optimizer state memory footprint than Adam-8D, a trend that inverts as model size increases. This is because the size of the embedding and lm-head matrices remains the same across model sizes because of a fixed vocabulary. For the XS model, these layers constitute up to 47% of model parameters and are optimized with 32-bit AdamW. The high memory cost for these layers offsets the savings achieved in the rest of the model.

6 CONCLUSIONS

In this paper, we introduced 8-bit Muon, a memory-efficient optimizer designed to address the problem of large memory footprints of LLMs. We build on the Muon optimizer and leverage blockwise quantization. One key finding is the robustness of Muon to types of quantization. Our results across pre-training and fine-tuning of large models show that our 8-bit Muon variants nearly matched the performance of the full-precision Muon. In terms of practical benefits, our method reduced the optimizer state memory by up to 86% compared to AdamW and 74% compared to full-precision Muon for models up to 1.6B-3B in size. Future work could include quantization to even lower bits, as well as combination with techniques like low-rank matrices.

REFERENCES

Kwangjun Ahn, Byron Xu, Natalie Abreu, and John Langford. Dion: Distributed orthonormalized updates. *arXiv preprint arXiv:2504.05295*, 2025.

Rohan Anil, Vineet Gupta, Tomer Koren, Kevin Regan, and Yoram Singer. Scalable second order optimization for deep learning. *arXiv preprint arXiv:2002.09018*, 2020.

Kayhan Behdin, Ayan Acharya, Aman Gupta, Qingquan Song, Siyu Zhu, Sathiya Keerthi, and Rahul Mazumder. Quantease: Optimization-based quantization for language models. *arXiv preprint arXiv:2309.01885*, 2023.

Jeremy Bernstein. Deriving muon. <https://jeremybernste.in/writing/deriving-muon>, 2025. Accessed: 2025-09-20.

Jeremy Bernstein and Laker Newhouse. Modular duality in deep learning. *arXiv preprint arXiv:2410.21265*, 2024a.

Jeremy Bernstein and Laker Newhouse. Old optimizer, new norm: An anthology. *arXiv preprint arXiv:2409.20325*, 2024b.

Rajendra Bhatia. *Matrix analysis*, volume 169. Springer Science & Business Media, 2013.

Dan Biderman, Jacob Portes, Jose Javier Gonzalez Ortiz, Mansheej Paul, Philip Greengard, Connor Jennings, Daniel King, Sam Havens, Vitaliy Chiley, Jonathan Frankle, et al. Lora learns less and forgets less. *arXiv preprint arXiv:2405.09673*, 2024.

Mark Chen, Jerry Tworek, Heewoo Jun, Qiming Yuan, Henrique Ponde De Oliveira Pinto, Jared Kaplan, Harri Edwards, Yuri Burda, Nicholas Joseph, Greg Brockman, et al. Evaluating large language models trained on code. *arXiv preprint arXiv:2107.03374*, 2021.

Karl Cobbe, Vineet Kosaraju, Mohammad Bavarian, Mark Chen, Heewoo Jun, Lukasz Kaiser, Matthias Plappert, Jerry Tworek, Jacob Hilton, Reiichiro Nakano, et al. Training verifiers to solve math word problems. *arXiv preprint arXiv:2110.14168*, 2021.

Jia Deng, Wei Dong, Richard Socher, Li-Jia Li, Kai Li, and Li Fei-Fei. Imagenet: A large-scale hierarchical image database. In *2009 IEEE conference on computer vision and pattern recognition*, pp. 248–255. Ieee, 2009.

Tim Dettmers, Mike Lewis, Sam Shleifer, and Luke Zettlemoyer. 8-bit optimizers via block-wise quantization. *arXiv preprint arXiv:2110.02861*, 2021.

Tim Dettmers, Artidoro Pagnoni, Ari Holtzman, and Luke Zettlemoyer. Qlora: Efficient finetuning of quantized llms. *arXiv preprint arXiv:2305.14314*, 2023.

Arthur Douillard, Qixuan Feng, Andrei A Rusu, Rachita Chhaparia, Yani Donchev, Adhiguna Kunoro, M Ranzato, Arthur Szlam, and Jiajun Shen. Diloco: Distributed low-communication training of language models, 2023. URL <https://arxiv.org/abs/2311.08105>.

Abhimanyu Dubey, Abhinav Jauhri, Abhinav Pandey, Abhishek Kadian, Ahmad Al-Dahle, Aiesha Letman, Akhil Mathur, Alan Schelten, Amy Yang, Angela Fan, et al. The llama 3 herd of models. *arXiv e-prints*, pp. arXiv–2407, 2024.

Elias Frantar, Saleh Ashkboos, Torsten Hoefer, and Dan Alistarh. Gptq: Accurate post-training quantization for generative pre-trained transformers. *arXiv preprint arXiv:2210.17323*, 2022.

Priya Goyal, Piotr Dollár, Ross Girshick, Pieter Noordhuis, Lukasz Wesolowski, Aapo Kyrola, Andrew Tulloch, Yangqing Jia, and Kaiming He. Accurate, large minibatch sgd: Training imagenet in 1 hour. *arXiv preprint arXiv:1706.02677*, 2017.

Aaron Grattafiori, Abhimanyu Dubey, Abhinav Jauhri, Abhinav Pandey, Abhishek Kadian, Ahmad Al-Dahle, Aiesha Letman, Akhil Mathur, and et al. The Llama 3 Herd of Models, November 2024. URL <http://arxiv.org/abs/2407.21783>. arXiv:2407.21783 [cs].

Kaiming He, Xiangyu Zhang, Shaoqing Ren, and Jian Sun. Deep residual learning for image recognition. In *Proceedings of the IEEE conference on computer vision and pattern recognition*, pp. 770–778, 2016.

Nicholas J Higham. *Functions of matrices: theory and computation*. SIAM, 2008.

Jordan Hoffmann, Sebastian Borgeaud, Arthur Mensch, Elena Buchatskaya, Trevor Cai, Eliza Rutherford, Diego de Las Casas, Lisa Anne Hendricks, Johannes Welbl, Aidan Clark, et al. Training compute-optimal large language models. *arXiv preprint arXiv:2203.15556*, 2022.

Edward J Hu, Yelong Shen, Phillip Wallis, Zeyuan Allen-Zhu, Yuanzhi Li, Shean Wang, Lu Wang, Weizhu Chen, et al. Lora: Low-rank adaptation of large language models. *ICLR*, 1(2):3, 2022.

Shengding Hu, Yuge Tu, Xu Han, Chaoqun He, Ganqu Cui, Xiang Long, Zhi Zheng, Yewei Fang, Yuxiang Huang, Weilin Zhao, et al. Minicpm: Unveiling the potential of small language models with scalable training strategies. *arXiv preprint arXiv:2404.06395*, 2024.

Keller Jordan et al. Muon: An optimizer for hidden layers in neural networks. <https://kellerjordan.github.io/posts/muon/>, 2024. Accessed 2025-09-18.

Jared Kaplan, Sam McCandlish, Tom Henighan, Tom B. Brown, Benjamin Chess, Rewon Child, Scott Gray, Alec Radford, Jeffrey Wu, and Dario Amodei. Scaling laws for neural language models. *CoRR*, abs/2001.08361, 2020. URL <https://arxiv.org/abs/2001.08361>.

Diederik P Kingma. Adam: A method for stochastic optimization. *arXiv preprint arXiv:1412.6980*, 2014.

Nathan Lambert, Jacob Morrison, Valentina Pyatkin, Shengyi Huang, Hamish Ivison, Faeze Brahman, Lester James V Miranda, Alisa Liu, Nouha Dziri, Shane Lyu, et al. Tulu 3: Pushing frontiers in open language model post-training. *arXiv preprint arXiv:2411.15124*, 2024.

Ren-Cang Li. New perturbation bounds for the unitary polar factor. *SIAM Journal on Matrix Analysis and Applications*, 16(1):327–332, 1995.

Ji Lin, Jiaming Tang, Haotian Tang, Shang Yang, Wei-Ming Chen, Wei-Chen Wang, Guangxuan Xiao, Xingyu Dang, Chuang Gan, and Song Han. Awq: Activation-aware weight quantization for on-device llm compression and acceleration. *Proceedings of machine learning and systems*, 6:87–100, 2024.

Jingyuan Liu, Jianlin Su, Xingcheng Yao, Zhejun Jiang, Guokun Lai, Yulun Du, Yidao Qin, Weixin Xu, Enzhe Lu, Junjie Yan, et al. Muon is scalable for llm training. *arXiv preprint arXiv:2502.16982*, 2025.

Zechun Liu, Barlas Oguz, Changsheng Zhao, Ernie Chang, Pierre Stock, Yashar Mehdad, Yangyang Shi, Raghuraman Krishnamoorthi, and Vikas Chandra. Llm-qat: Data-free quantization aware training for large language models. *arXiv preprint arXiv:2305.17888*, 2023.

Ilya Loshchilov and Frank Hutter. Fixing weight decay regularization in adam. *CoRR*, abs/1711.05101, 2017. URL <http://arxiv.org/abs/1711.05101>.

Guilherme Penedo, Hynek Kydlíček, Anton Lozhkov, Margaret Mitchell, Colin A Raffel, Leandro Von Werra, Thomas Wolf, et al. The fineweb datasets: Decanting the web for the finest text data at scale. *Advances in Neural Information Processing Systems*, 37:30811–30849, 2024.

Alec Radford, Jeffrey Wu, Rewon Child, David Luan, Dario Amodei, Ilya Sutskever, et al. Language models are unsupervised multitask learners. *OpenAI blog*, 1(8):9, 2019.

Samyam Rajbhandari, Jeff Rasley, Olatunji Ruwase, and Yuxiong He. Zero: Memory optimizations toward training trillion parameter models. In *SC20: International Conference for High Performance Computing, Networking, Storage and Analysis*, pp. 1–16. IEEE, 2020.

Ishaan Shah, Anthony M Polloreno, Karl Stratos, Philip Monk, Adarsh Chaluvaraju, Andrew Hojel, Andrew Ma, Anil Thomas, Ashish Tanwer, Darsh J Shah, et al. Practical efficiency of muon for pretraining. *arXiv preprint arXiv:2505.02222*, 2025.

Noam Shazeer and Mitchell Stern. Adafactor: Adaptive learning rates with sublinear memory cost. In *International Conference on Machine Learning*, pp. 4596–4604. PMLR, 2018.

Mohammad Shoeybi, Mostofa Patwary, Raul Puri, Patrick LeGresley, Jared Casper, and Bryan Catanzaro. Megatron-lm: Training multi-billion parameter language models using model parallelism. *arXiv preprint arXiv:1909.08053*, 2019.

Jianlin Su, Murtadha Ahmed, Yu Lu, Shengfeng Pan, Wen Bo, and Yunfeng Liu. Roformer: Enhanced transformer with rotary position embedding. *Neurocomputing*, 568:127063, 2024.

Kimi Team, Yifan Bai, Yiping Bao, Guanduo Chen, Jiahao Chen, Ningxin Chen, Ruijue Chen, Yanru Chen, Yuankun Chen, Yutian Chen, et al. Kimi k2: Open agentic intelligence. *arXiv preprint arXiv:2507.20534*, 2025.

Benjamin Thérien, Xiaolong Huang, Irina Rish, and Eugene Belilovsky. Muloco: Muon is a practical inner optimizer for diloco. *arXiv preprint arXiv:2505.23725*, 2025.

Albert Tseng, Jerry Chee, Qingyao Sun, Volodymyr Kuleshov, and Christopher De Sa. Quip#: Even better llm quantization with hadamard incoherence and lattice codebooks. *arXiv preprint arXiv:2402.04396*, 2024.

Nikhil Vyas, Depen Morwani, Rosie Zhao, Mujin Kwun, Itai Shapira, David Brandfonbrener, Lucas Janson, and Sham Kakade. Soap: Improving and stabilizing shampoo using adam. *arXiv preprint arXiv:2409.11321*, 2024.

Aohan Zeng, Xin Lv, Qinkai Zheng, Zhenyu Hou, Bin Chen, Chengxing Xie, Cunxiang Wang, Da Yin, Hao Zeng, Jiajie Zhang, et al. Glm-4.5: Agentic, reasoning, and coding (arc) foundation models. *arXiv preprint arXiv:2508.06471*, 2025.

Jiawei Zhao, Zhenyu Zhang, Beidi Chen, Zhangyang Wang, Anima Anandkumar, and Yuandong Tian. Galore: Memory-efficient llm training by gradient low-rank projection. *arXiv preprint arXiv:2403.03507*, 2024.

Yanli Zhao, Andrew Gu, Rohan Varma, Liang Luo, Chien-Chin Huang, Min Xu, Less Wright, Hamid Shojanazeri, Myle Ott, Sam Shleifer, et al. Pytorch fsdp: experiences on scaling fully sharded data parallel. *arXiv preprint arXiv:2304.11277*, 2023.

A APPENDIX

A.1 TRAINING HYPERPARAMETER DETAILS

A.1.1 IMAGENET TRAINING DETAILS

We trained ResNet-50 on ImageNet for 90 epochs using two H100 GPUs with PyTorch Distributed-DataParallel. The schedule was the standard 90-epoch multi-step regime with learning rate decays at epochs 30, 60, and 80. For SGD with momentum we used a batch size of 128 per GPU (256 total), momentum 0.9, and weight decay 10^{-4} . For AdamW we used a learning rate of 3×10^{-3} and weight decay 10^{-2} . Hyperparameters were held fixed across FP32 and quantized runs. Training images were augmented with random resized crops to 224×224 and random horizontal flips. At evaluation time, images were resized to 256 pixels on the short side and center-cropped to 224×224 , followed by normalization with the standard ImageNet mean and variance.

Model size	Parameters	d_{model}	n_{layers}	n_{heads}	FF Ratio
XS	97M	576	10	12	4
Small	162M	768	12	12	4
Medium	405M	1024	24	16	4
XL	1.6B	1600	48	25	4

Table 6: Model sizes used for the pre-training task.

In the quantized variants, optimizer states were stored in 8-bit linear form with per-tensor scaling (Definition 1 applied layer-wise). For SGD with momentum, only the momentum buffer was quantized. For AdamW, both the first- and second-moment estimates were quantized. At each step, stored values were dequantized for computation, updated, and then requantized. Model weights, gradients, and activations were always maintained in FP32.

Figure 4 reports validation accuracy during training. Quantized SGD matches the FP32 baseline throughout. AdamW with FP32 optimizer states achieves slightly lower accuracy, while the quantized AdamW variant diverged immediately and is not shown.

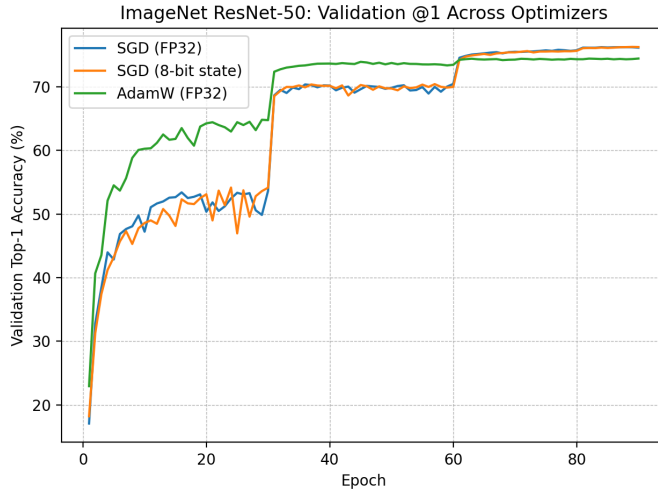


Figure 4: Validation top-1 accuracy on ImageNet for ResNet-50. Quantized SGD overlaps with the FP32 baseline. AdamW with FP32 states underperforms slightly, while the quantized AdamW variant diverged at the first step and is not shown.

A.1.2 PRE-TRAINING DETAILS

We train 4 GPT-style models on 2B to 4B tokens using 8 H100 GPUs with PyTorch Distributed DataParallel (DDP). A summary of the model architectures used is described in Table 6.

Model sizes up to 405M were trained on 2B tokens with a learning rate of $3 \cdot 10^{-4}$ with a per-GPU batch size of 16 samples or 32768 tokens. We purposely use the same number of samples per optimizer step for all model sizes despite lower Model FLOPs Utilization to have a fair comparison between model sizes. The same logic is applied to the XL model, which is trained with a local batch size of 2 and 8 gradient accumulation steps for all optimizer variants. A summary of the training hyperparameters used for training is shown in Table 7

B MUON ALGORITHMS

Algos 1, 2 and 3 represent vanilla Muon (Jordan et al., 2024), Muon (Liu et al., 2025) and Quantized Muon. **Note** The algos use small-case vector notation.

Model size	LR	Local BS	Grad. Acc. Steps	Global BS
XS	$3 \cdot 10^{-4}$	32768	1	262144
Small	$3 \cdot 10^{-4}$	32768	1	262144
Medium	$3 \cdot 10^{-4}$	32768	1	262144
XL	$2 \cdot 10^{-4}$	4096	8	262144

Table 7: Training configuration for the pre-training task. LR refers to the learning rate, and BS refers to the batch size. Both local and global batch sizes reported are in number of tokens, as all models were trained with a context length of 2048.

Algorithm 1 Vanilla Muon (using $\theta, \mathbf{g}, \mathbf{m}$; NS-orthogonalized momentum for 2D hidden-layer params)

```

1: Input: step size  $\alpha$ , momentum  $\beta \in [0, 1]$ , NS steps  $T$  (default 5),  $\epsilon > 0$ 
2: Initialize:  $\theta^{(0)}, \tilde{\mathbf{m}}^{(0)} = \mathbf{0}$ 
3: for  $t = 1, 2, \dots$  do
4:    $\mathbf{g}^{(t)} \leftarrow \nabla f_t(\theta^{(t-1)})$ 
5:    $\tilde{\mathbf{m}}^{(t)} \leftarrow \beta \tilde{\mathbf{m}}^{(t-1)} + (1 - \beta) \mathbf{g}^{(t)}$   $\triangleright$  SGD-style momentum before orthogonalization
6:   for each 2D hidden-layer parameter block  $\theta \subset \theta$  do
7:      $\Delta \leftarrow \text{NS}(\tilde{\mathbf{m}}^{(t)}[\theta], T, \epsilon)$   $\triangleright$  Orthogonalize update
8:      $\theta \leftarrow \theta - \alpha \Delta$ 
9:   end for
10: end for

```

Algorithm 2 Muon (using $\theta, \mathbf{g}, \mathbf{m}$; NS-orthogonalized momentum for 2D hidden-layer params)

```

1: Input: step size  $\alpha$ , momentum  $\beta \in [0, 1]$ , weight decay  $\lambda \geq 0$ , NS steps  $T$  (default 5),  $\epsilon > 0$ 
2: Initialize:  $\theta^{(0)}, \tilde{\mathbf{m}}^{(0)} = \mathbf{0}$ 
3: for  $t = 1, 2, \dots$  do
4:    $\mathbf{g}^{(t)} \leftarrow \nabla f_t(\theta^{(t-1)})$ 
5:    $\tilde{\mathbf{m}}^{(t)} \leftarrow \beta \tilde{\mathbf{m}}^{(t-1)} + (1 - \beta) \mathbf{g}^{(t)}$   $\triangleright$  SGD-style momentum before orthogonalization
6:   for each 2D hidden-layer parameter block  $\theta \subset \theta$  (with dimensions  $m, n$ ) do
7:      $\Delta \leftarrow \text{NS}(\tilde{\mathbf{m}}^{(t)}[\theta], T, \epsilon)$   $\triangleright$  Orthogonalize update
8:      $\theta \leftarrow (1 - \alpha \lambda) \theta - 0.2 \alpha \sqrt{\max(m, n)} \Delta$ 
9:   end for
10: end for

```

Algorithm 3 Quantized Muon (using $\theta, \mathbf{g}, \mathbf{m}$; NS-orthogonalized momentum for 2D hidden-layer params)

```

1: Input: step size  $\alpha$ , momentum  $\beta \in [0, 1]$ , weight decay  $\lambda \geq 0$ , NS steps  $T, \epsilon > 0$ , quantization
   params (mode, bits  $B$ )
2: Initialize:  $\theta^{(0)}$ , quantized momentum state  $(\mathbf{z}^{(0)}, \mathbf{s}^{(0)}) = (\mathbf{0}, \mathbf{0})$ 
3: for  $t = 1, 2, \dots$  do
4:    $\mathbf{g}^{(t)} \leftarrow \nabla f_t(\theta^{(t-1)})$ 
5:   for each 2D hidden-layer parameter block  $\theta \subset \theta$  (with dimensions  $m, n$ ) do
6:      $\tilde{\mathbf{m}}^{(t-1)} \leftarrow \text{DEQUANTIZE}(\mathbf{z}^{(t-1)}[\theta], \mathbf{s}^{(t-1)}[\theta])$   $\triangleright$  Dequantize saved momentum state
7:      $\mathbf{m}^{(t)} \leftarrow \beta \tilde{\mathbf{m}}^{(t-1)} + \mathbf{g}^{(t)}[\theta]$   $\triangleright$  Update momentum with current gradient
8:      $\mathbf{u}^{(t)} \leftarrow \text{NS}(\mathbf{m}^{(t)}, T, \epsilon)$   $\triangleright$  Orthogonalize momentum for the update
9:      $\theta \leftarrow (1 - \alpha \lambda) \theta - 0.2 \alpha \sqrt{\max(m, n)} \mathbf{u}^{(t)}$   $\triangleright$  Update parameters
10:     $(\mathbf{z}^{(t)}[\theta], \mathbf{s}^{(t)}[\theta]) \leftarrow \text{QUANTIZE}(\mathbf{m}^{(t)})$   $\triangleright$  Quantize and save new momentum state
11:   end for
12: end for

```

C QUANTIZATION ERROR BOUNDS

In this appendix we formalize the 8-bit linear quantization operator and provide detailed proofs of the error bounds for Adam and SGD with momentum under quantization. We adopt the same notation as in Algorithm 4: \mathbf{g} is the stochastic gradient, \mathbf{m} and \mathbf{v} are the first- and second-moment accumulators, \mathbf{g}^2 denotes the entrywise square, $\sqrt{\mathbf{v}}$ denotes the entrywise square root, and $\text{vec}(\mathbf{M})$ denotes the vectorization of \mathbf{M} .

C.1 QUANTIZATION OPERATOR

Definition 1 (*Linear quantization*). For a given vector $\mathbf{x} \in \mathbb{R}^d$ denoting the optimizer state of some algorithm, the 8-bit linear quantization is denoted by $Q : \mathbb{R}^d \rightarrow \mathbb{R}^d$, where:

$$[Q(\mathbf{x})]_i = \frac{\|\mathbf{x}\|_\infty}{127} \cdot \text{round} \left(\frac{127 \cdot \mathbf{x}_i}{\|\mathbf{x}\|_\infty} \right).$$

That is, each coordinate of \mathbf{x} is mapped to the nearest grid point in a uniform partition of $[-\|\mathbf{x}\|_\infty, \|\mathbf{x}\|_\infty]$ into 256 representable levels (corresponding to signed 8-bit integers from -128 to 127), then rescaled back to floating point. This is the standard max-abs scaling scheme used in prior 8-bit quantization work. Note that, although we work over the reals, this definition effectively models the quantization and de-quantization steps applied to optimizer states between iterations.

C.2 PROOFS

C.2.1 PROOF OF THEOREM 1

Proof

As stated in the theorem, we work at the first step ($t = 1$) and suppress iterate superscripts for notational clarity. By the moment definitions in Algorithm 4, we have $\mathbf{m} = \mathbf{g}$ and $\mathbf{v} = \mathbf{g}^2$ (entrywise), so for each coordinate i we have $\sqrt{\mathbf{v}_i} = |\mathbf{g}_i|$. We first lower bound the per-coordinate deviation $\left| \frac{\mathbf{m}_i}{\sqrt{\mathbf{v}_i} + \epsilon} - \frac{Q(\mathbf{m}_i)}{\sqrt{Q(\mathbf{v}_i)} + \epsilon} \right|$ and then sum over i .

$$\begin{aligned} \mathbb{P} \left(\left(\frac{\mathbf{m}_i}{\sqrt{\mathbf{v}_i} + \epsilon} - \frac{Q(\mathbf{m}_i)}{\sqrt{Q(\mathbf{v}_i)} + \epsilon} \right)^2 \geq t^2 \right) &= \mathbb{P} \left(\left| \frac{\mathbf{m}_i}{\sqrt{\mathbf{v}_i} + \epsilon} - \frac{Q(\mathbf{m}_i)}{\sqrt{Q(\mathbf{v}_i)} + \epsilon} \right| \geq t \right) \\ &\geq \mathbb{P} \left(\frac{|\mathbf{g}_i| - \|\mathbf{g}\|_\infty/127}{\sqrt{Q(\mathbf{v}_i)} + \epsilon} - \frac{|\mathbf{g}_i|}{\sqrt{\mathbf{v}_i} + \epsilon} \geq t \text{ and } \mathbf{v}_i \geq Q(\mathbf{v}_i) \right) \end{aligned}$$

Note that $\sqrt{\mathbf{v}_i} = \sqrt{\mathbf{g}_i^2} = |\mathbf{g}_i|$ and $Q(\mathbf{v}_i) = 0$ implies $\mathbf{v}_i \geq Q(\mathbf{v}_i)$. Hence, following from above,

$$\begin{aligned} \mathbb{P} \left(\left(\frac{\mathbf{m}_i}{\sqrt{\mathbf{v}_i} + \epsilon} - \frac{Q(\mathbf{m}_i)}{\sqrt{Q(\mathbf{v}_i)} + \epsilon} \right)^2 \geq t^2 \right) &\geq \mathbb{P} \left(\frac{|\mathbf{g}_i| - \|\mathbf{g}\|_\infty/127}{\epsilon} - \frac{|\mathbf{g}_i|}{|\mathbf{g}_i| + \epsilon} \geq t \text{ and } Q(\mathbf{v}_i) = 0 \right) \\ &\geq \mathbb{P} \left(\frac{|\mathbf{g}_i| - \|\mathbf{g}\|_\infty/127}{\epsilon} - 1 \geq t \text{ and } Q(\mathbf{v}_i) = 0 \right) \end{aligned}$$

Define the event $E_i := \{ \frac{\|\mathbf{g}\|_\infty}{60} < |\mathbf{g}_i| \leq \frac{\|\mathbf{g}\|_\infty}{16} \}$. By the assumption of the theorem, $\mathbb{P}(E_i) \geq \nu$, and on E_i we have both $Q(\mathbf{v}_i) = 0$ and

$$\begin{aligned} \frac{|\mathbf{g}_i| - \|\mathbf{g}\|_\infty/127}{\epsilon} &\geq \frac{\|\mathbf{g}\|_\infty/60 - \|\mathbf{g}\|_\infty/127}{\epsilon} \\ &\geq \frac{\|\mathbf{g}\|_\infty}{128\epsilon}. \end{aligned}$$

Since $\|\mathbf{g}\|_\infty \geq g_\infty$ almost surely and $g_\infty \geq 256\epsilon$,

$$\begin{aligned}\frac{\|\mathbf{g}\|_\infty}{128\epsilon} - 1 &\geq \frac{g_\infty}{128\epsilon} - 1 \\ &\geq \frac{1}{2} \cdot \frac{g_\infty}{128\epsilon} = \frac{g_\infty}{256\epsilon}.\end{aligned}$$

Set $\tau_0 := \frac{g_\infty}{256\epsilon}$. Then, for $t = \tau_0$,

$$\begin{aligned}\mathbb{P}\left(\left|\frac{\mathbf{m}_i}{\sqrt{\mathbf{v}_i} + \epsilon} - \frac{Q(\mathbf{m}_i)}{\sqrt{Q(\mathbf{v}_i)} + \epsilon}\right| \geq t\right) &\geq \mathbb{P}(E_i) \\ &\geq \nu.\end{aligned}$$

Therefore, using $\mathbb{E}[X^2] \geq t^2\mathbb{P}(X \geq t)$ for nonnegative X ,

$$\mathbb{E}\left[\left(\frac{\mathbf{m}_i}{\sqrt{\mathbf{v}_i} + \epsilon} - \frac{Q(\mathbf{m}_i)}{\sqrt{Q(\mathbf{v}_i)} + \epsilon}\right)^2\right] \geq \nu \tau_0^2 = \nu \frac{g_\infty^2}{(256\epsilon)^2}.$$

Summing over $i = 1, \dots, d$ and using $\boldsymbol{\theta}^{(1)} - \tilde{\boldsymbol{\theta}}^{(1)} = \alpha\left(\frac{\mathbf{m}}{\sqrt{\mathbf{v}} + \epsilon} - \frac{Q(\mathbf{m})}{\sqrt{Q(\mathbf{v})} + \epsilon}\right)$,

$$\mathbb{E}\|\boldsymbol{\theta}^{(1)} - \tilde{\boldsymbol{\theta}}^{(1)}\|_2^2 \geq \alpha^2 d \nu \frac{g_\infty^2}{(256\epsilon)^2}.$$

■

C.2.2 PROOF OF THEOREM 2

Proof We compare the two updates and isolate the effect of quantizing the momentum. The gradient terms cancel, leaving

$$\begin{aligned}\tilde{\boldsymbol{\theta}}^{(t+1)} - \boldsymbol{\theta}^{(t+1)} &= -\eta(\mathbf{g}^{(t)} + \rho Q(\mathbf{m}^{(t)})) + \eta(\mathbf{g}^{(t)} + \rho \mathbf{m}^{(t)}) \\ &= -\eta\rho(Q(\mathbf{m}^{(t)}) - \mathbf{m}^{(t)}).\end{aligned}$$

Taking squared norms and expanding coordinatewise yields

$$\|\tilde{\boldsymbol{\theta}}^{(t+1)} - \boldsymbol{\theta}^{(t+1)}\|_2^2 = \eta^2 \rho^2 \sum_{i=1}^d \left(Q(\mathbf{m}^{(t)})_i - \mathbf{m}_i^{(t)}\right)^2.$$

By Definition 1, each coordinate is perturbed by at most $\|\mathbf{m}^{(t)}\|_\infty/127$, i.e., $|Q(\mathbf{m}^{(t)})_i - \mathbf{m}_i^{(t)}| \leq \|\mathbf{m}^{(t)}\|_\infty/127$. Applying this inside the sum gives

$$\begin{aligned}\|\tilde{\boldsymbol{\theta}}^{(t+1)} - \boldsymbol{\theta}^{(t+1)}\|_2^2 &\leq \eta^2 \rho^2 \sum_{i=1}^d \left(\|\mathbf{m}^{(t)}\|_\infty/127\right)^2 \\ &= d \eta^2 \rho^2 \left(\|\mathbf{m}^{(t)}\|_\infty/127\right)^2,\end{aligned}$$

which is the claimed bound. ■

C.2.3 PROOF OF THEOREM 3

Proof From the two updates,

$$\widetilde{\mathbf{W}}^{(t)} - \mathbf{W}^{(t)} = -\alpha(\widetilde{\mathbf{O}}^{(t)} - \mathbf{O}^{(t)}) \Rightarrow \|\widetilde{\mathbf{W}}^{(t)} - \mathbf{W}^{(t)}\|_{\text{F}} = \alpha \|\widetilde{\mathbf{O}}^{(t)} - \mathbf{O}^{(t)}\|_{\text{F}}.$$

The momentum matrices $\mathbf{M}^{(t)}$ and $\widetilde{\mathbf{M}}^{(t)}$ are assumed to be full column rank with $\sigma_{\min}(\mathbf{M}^{(t)}), \sigma_{\min}(\widetilde{\mathbf{M}}^{(t)}) \geq s > 0$. For full-column-rank matrices, the (rectangular) polar-factor map satisfies

$$\|\widetilde{\mathbf{O}}^{(t)} - \mathbf{O}^{(t)}\|_F \leq \frac{2}{\sigma_{\min}(\mathbf{M}^{(t)}) + \sigma_{\min}(\widetilde{\mathbf{M}}^{(t)})} \|\widetilde{\mathbf{M}}^{(t)} - \mathbf{M}^{(t)}\|_F \leq \frac{1}{s} \|\widetilde{\mathbf{M}}^{(t)} - \mathbf{M}^{(t)}\|_F,$$

(see (Bhatia, 2013, Thm. VII.5.1(a)) and its extension to full column rank in (Li, 1995, Thm. 2)). Hence

$$\|\widetilde{\mathbf{W}}^{(t)} - \mathbf{W}^{(t)}\|_F \leq \alpha \frac{1}{s} \|\widetilde{\mathbf{M}}^{(t)} - \mathbf{M}^{(t)}\|_F = \alpha \frac{\beta}{s} \|Q(\mathbf{M}^{(t-1)}) - \mathbf{M}^{(t-1)}\|_F.$$

By Definition 1, each entry changes by at most $\|\text{vec}(\mathbf{M}^{(t-1)})\|_\infty/127$, so $\|Q(\mathbf{M}^{(t-1)}) - \mathbf{M}^{(t-1)}\|_F^2 \leq d(\|\text{vec}(\mathbf{M}^{(t-1)})\|_\infty/127)^2$. Squaring both sides completes the proof. \blacksquare

C.3 ADAM ALGORITHM

For completeness, we reproduce the base Adam algorithm below (Algorithm 1 in Kingma (2014)).

Algorithm 4 Adam (using $\theta, \mathbf{g}, \mathbf{m}, \mathbf{v}$)

- 1: **Input:** step size α , decay rates $\beta_1, \beta_2 \in [0, 1)$, $\epsilon > 0$
- 2: **Initialize:** $\theta^{(0)}, \tilde{\mathbf{m}}^{(0)} = \mathbf{0}, \tilde{\mathbf{v}}^{(0)} = \mathbf{0}$
- 3: **for** $t = 1, 2, \dots$ **do**
- 4: $\mathbf{g}^{(t)} \leftarrow \nabla f_t(\theta^{(t-1)})$
- 5: $\tilde{\mathbf{m}}^{(t)} \leftarrow \beta_1 \tilde{\mathbf{m}}^{(t-1)} + (1 - \beta_1) \mathbf{g}^{(t)}$
- 6: $\tilde{\mathbf{v}}^{(t)} \leftarrow \beta_2 \tilde{\mathbf{v}}^{(t-1)} + (1 - \beta_2) (\mathbf{g}^{(t)})^2$
- 7: $\mathbf{m}^{(t)} \leftarrow \tilde{\mathbf{m}}^{(t)} / (1 - \beta_1^t)$
- 8: $\mathbf{v}^{(t)} \leftarrow \tilde{\mathbf{v}}^{(t)} / (1 - \beta_2^t)$
- 9: $\theta^{(t)} \leftarrow \theta^{(t-1)} - \alpha \mathbf{m}^{(t)} / (\sqrt{\mathbf{v}^{(t)}} + \epsilon)$
- 10: **end for**

C.4 EXACT MUON OPTIMIZER

For completeness, we provide the update formula for the exact Muon algorithm (without weight decay) here. As opposed to eqn. (1), this formula uses the exact polar factor $\mathbf{O} = \mathbf{U}^{(t)} \mathbf{V}^{(t)\top}$

$$\begin{aligned} \mathbf{M}^{(t)} &:= \beta \mathbf{M}^{(t-1)} + \mathbf{G}_t, \\ \mathbf{M}^{(t)} &= \mathbf{U}^{(t)} \mathbf{S}^{(t)} \mathbf{V}^{(t)\top} \text{ (thin SVD)}, \\ \mathbf{O}^{(t)} &:= \mathbf{U}^{(t)} \mathbf{V}^{(t)\top}, \\ \mathbf{W}^{(t)} &= \mathbf{W}^{(t-1)} - \alpha \mathbf{O}^{(t)}. \end{aligned} \tag{4}$$

In the quantized variant, only the previous momentum is quantized and then de-quantized, leading to the following updates where Q is defined in Definition 1:

$$\begin{aligned} \widetilde{\mathbf{M}}^{(t)} &:= \beta Q(\mathbf{M}^{(t-1)}) + \mathbf{G}_t, \\ \widetilde{\mathbf{M}}^{(t)} &= \widetilde{\mathbf{U}}^{(t)} \widetilde{\mathbf{S}}^{(t)} \widetilde{\mathbf{V}}^{(t)\top} \text{ (thin SVD)}, \\ \widetilde{\mathbf{O}}^{(t)} &:= \widetilde{\mathbf{U}}^{(t)} \widetilde{\mathbf{V}}^{(t)\top}, \\ \widetilde{\mathbf{W}}^{(t)} &= \mathbf{W}^{(t-1)} - \alpha \widetilde{\mathbf{O}}^{(t)}. \end{aligned} \tag{5}$$